AD-A137 744 MEASUREMENTS OF THE NEAR WAKE OF AN AIRFOIL IN UNSTEADY FLOW(U) MASSACHUSETTS INST OF TECH CAMBRIDGE DEPT OF AERONAUTICS AND A... E E COVERT ET AL. JAN 83 1/1

UNCLASSIFIED AFOSR-TR-84-0029 AFOSR-80-0282 F/G 20/4 NL

END

FILMED

3-84

DTIC

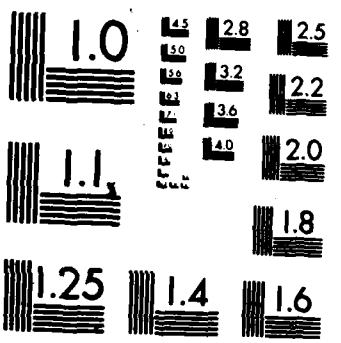

UNCLASSIFIED

SECURITY CLASSIFICATION OF THIS PAGE (When Data Entered)

REPORT DOCUMENTATION PAGE

READ INSTRUCTIONS BEFORE COMPLETING FORM

1. REPORT NUMBER	2. GOVT ACCESSION NO.	3. RECIPIENT'S CATALOG NUMBER
AFOSR-TR- 84-0029	AD-A137744	

4. TITLE (and Subtitle)
MEASUREMENTS OF THE NEAR WAKE OF AN AIRFOIL IN UNSTEADY FLOW

5. TYPE OF REPORT & PERIOD COVERED
INTERIM

6. PERFORMING ORG. REPORT NUMBER

7. AUTHOR(s)
E E COVERT
P F LORBER
C M VACZY

8. CONTRACT OR GRANT NUMBER(s)
AFOSR-80-0282

9. PERFORMING ORGANIZATION NAME AND ADDRESS
MASSACHUSETTS INSTITUTE OF TECHNOLOGY
DEPARTMENT OF AERONAUTICS & ASTRONAUTICS
CAMBRIDGE, MA 02139

10. PROGRAM ELEMENT, PROJECT, TASK AREA & WORK UNIT NUMBERS
61102F
2307/A2

11. CONTROLLING OFFICE NAME AND ADDRESS
AIR FORCE OFFICE OF SCIENTIFIC RESEARCH/NA
BOLLING AFB, DC 20332

12. REPORT DATE
January 1983

13. NUMBER OF PAGES
11

14. MONITORING AGENCY NAME & ADDRESS(if different from Controlling Office)

15. SECURITY CLASS. (of this report)
Unclassified

15a. DECLASSIFICATION/DOWNGRADING SCHEDULE

16. DISTRIBUTION STATEMENT (of this Report)
Approved for Public Release; Distribution Unlimited.

17. DISTRIBUTION STATEMENT (of the abstract entered in Block 20, if different from Report)

18. SUPPLEMENTARY NOTES
Proceedings of the Aerospace Sciences Meeting, 21st Reno, Nevada, 10-13 Jan 1983, The American Institute of Aeronautics and Astronautics 1983

19. KEY WORDS (Continue on reverse side if necessary and identify by block number)
FLUID MECHANICS
HOT-WIRE ANEMOMETER
UNSTEADY AERODYNAMICS
AIRFOIL AERODYNAMICS
WAKE FLOW
FLOW VELOCITIES

20. ABSTRACT (Continue on reverse side if necessary and identify by block number)
A series of measurements has been made of the velocities in the near wake of an airfoil in an unsteady flow generated by rotating an elliptic cylinder near the trailing edge. Ensemble averages of the tangential and normal velocity components and of 3 Reynolds stresses were determined for reduced frequencies based on semichord up to 6.4, angles of attack of 0 and 10 degrees, Reynolds numbers of 700,000 and 1,450,000, and chordwise positions $1.025 \leq x/c \leq 1.2$. In this region the airfoil wake is distinct from the wake of the elliptic cylinder. The mean and unsteady velocities and Reynolds

DD FORM 1 JAN 73 1473 EDITION OF 1 NOV 65 IS OBSOLETE

UNCLASSIFIED

SECURITY CLASSIFICATION OF THIS PAGE (When Data Entered)

stresses diffuse rapidly so that the distinction between the contributions due to the two boundary layers on the airfoil surfaces, apparent at x/c=1.025, has largely disappeared by x/c≈1.20.

AIAA'83

AIAA-83-0127
Measurements of the Near Wake of an Airfoil in Unsteady Flow

E.E. Covert, P.F. Lorber and C.M. Vaczy,
Massachusetts Institute of Technology,
Cambridge, MA

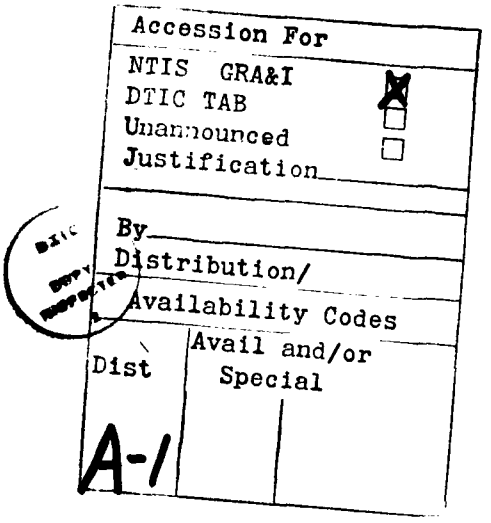

AIAA 21st Aerospace Sciences Meeting

January 10-13, 1983/Reno, Nevada

MEASUREMENTS OF THE NEAR WAKE OF AN AIRFOIL IN UNSTEADY FLOW

E.E.Covert*, P.F.Lorber**, and C.M.Vaczy**

Department of Aeronautics and Astronautics
Massachusetts Institute of Technology
Cambridge, MA 02139

Abstract

A series of measurements has been made of the velocities in the near wake of an airfoil in an unsteady flow generated by rotating an elliptic cylinder near the trailing edge. Ensemble averages of the tangential and normal velocity components and of 3 Reynolds stresses were determined for reduced frequencies based on semichord up to 6.4, angles of attack of 0 and 10 degrees, Reynolds numbers of 700,000 and 1,450,000, and chordwise positions $1.025<x/c<1.2$. In this region the airfoil wake is distinct from the wake of the elliptic cylinder. The mean and unsteady velocities and Reynolds stresses diffuse rapidly so that the distinction between the contributions due to the two boundary layers on the airfoil surfaces, apparent at x/c=1.025, has largely disappeared by x/c=1.20.

Nomenclature

c airfoil chord
k reduced frequency, $\omega c/2U_\infty$
Re Reynolds number based on airfoil chord
U_e mean velocity above the shear layer
U_∞ freestream velocity
u velocity component in the x direction
v velocity component in the y direction
x distance from the leading edge along the chord line
y distance normal to the chord line

α airfoil angle of attack
ω oscillation frequency in radians/sec

$\bar{u}$ time average of u
$\langle u \rangle$ ensemble average of u
$\tilde{u}$ periodic component of zero mean, $\tilde{u}=\langle u \rangle - \bar{u}$
u′ aperiodic component, $u'=u-\langle u \rangle$

note that $\overline{\tilde{u}}=\overline{u'}=\langle u' \rangle=0$

* Professor of Aeronautics and Astronautics, Fellow AIAA
** Research Assistant, Student Member AIAA

Introduction

Unsteady flows over airfoils are characteristic of many aerodynamic applications, including helicopter rotors, aircraft wing and control surfaces subject to maneuver or gust loading, and gas turbine engine stages. The current paper presents data on the turbulent wake of an airfoil in an unsteady flow. Airfoil unsteady pressure data for this experimental configuration were discussed in reference 1, while some results for the unsteady turbulent boundary layer at various adverse pressure gradients were given in reference 2.

Currently, experimental, numerical, and analytical work on turbulent boundary layers and wakes is being undertaken at many levels of flow complexity. For example, the detailed study of the wake of a steady flat plate is still in progress (3,4). For the more complex situation of the steady wake behind an airfoil, considerable work has been reported recently, both experimental (5,6), and numerical (7,8). The effect on the wake of rotation and flow curvature, such as is found in turbomachine stages, has also been examined, primarily with regard to mean flow quantities (9,10).

Unsteady wake experiments and analysis are less common. Satyanarayana (11) studied the tangential velocity profiles in the wake of an airfoil in unsteady flow generated by oscillation of the wind tunnel walls. Ho and Chen (12,13) measured velocity and turbulent stress profiles and integrated to determine steamlines behind a plunging airfoil. DeRuyck and Hirsh (14) measured profiles behind a pitching airfoil over a relatively wide range of frequency, mean incidence, and distance downstream.

Experiment

As a description of the experimental apparatus and procedure has been given elsewhere (1,2), only a summary is required here. A 50.8 cm. chord NACA 0012 airfoil is located between vertical sidewalls in a low speed (1 to 90 mps) wind tunnel. The majority of the data reported here were taken at a Reynolds number based on

chord of 700,000. Two unsteady flow conditions were tested. The first consisted of mounting the airfoil at zero angle of attack, with a rotating elliptic cylinder (semiaxes of 0.136 and 0.061 chord) located behind and beneath the airfoil trailing edge (axis of rotation at x/c=1.175, y/c=-.275). The second rotated the airfoil to 10 degrees angle of attack and moved the elliptic cylinder axis to x/c=1.120, y/c=-.190. Steady state data were taken for 3 cases: no elliptic cylinder, ellipse major axis horizontal (parallel to the freestream), and major axis vertical. Unsteady data were taken for reduced frequencies based on semichord of k=0.5, 2.0, and 6.4 at zero angle of attack, and at k=0.5, 2.0, and 3.9 at 10 degrees.

A constant temperature cross hot wire was moved perpendicular to the airfoil chord at five locations along the chord line, x/c=1.025, 1.05, 1.10, 1.20, and 1.40. Ensemble averages based on the ellipse rotation period were determined digitally for the five quantities u, v, u'u', v'v', and u'v'. Depending on the ratio of the periodic signal to the aperiodic 'noise', from 100 to 2048 periods were used to form the average. These data were stored and later Fourier transformed. Data are reported here for the mean and for the amplitude and phase lag of the fundamental harmonic (twice the rotation frequency). Phase lag is normalized so that 720 degrees corresponds to one ellipse rotation, and 0 phase lag implies that the minimum of the quantity occurs when the ellipse major axis is horizontal. Estimated experimental accuracies are as follows: Mean velocities to ±1% of U_∞. Mean Reynolds stresses to ±5% of the local value. Periodic velocity amplitudes to ±3% of the extenal amplitude, and phase lags to ±3 degrees. Unsteady Reynolds stress amplitudes to ±10% of the local value. A side view of the experiment is combined with a block diagram of the data acquisition system in figure 1.

Discussion of Results

As is common in unsteady aerodynamics due to the large number of relevant parameters (frequency, Reynolds number, angle of attack, and measurement location), the present experiment has produced an abundance of data. Even after data for all measurement locations in (x,y) have been condensed onto single plots, 109 figures would be required to present means and fundamental harmonic amplitudes for the 5 measured quantities and phase lags for 2 quantities (u and v). Therefore only a sample of the results will be given.

Mean tangential velocity profiles for steady conditions at zero angle of attack are shown in figures 2 and 3. Velocities are normalized by the mean velocity at the maximum y station for each x location. Heights are measured normal to the chord line and nondimensionalized by the airfoil chord. The velocity field may be interpreted as a superposition of the rapidly varying velocity deficit in the airfoil wake and the more slowly varying nonuniform flow due to the steady ellipse. Calculations based upon the potential flow about an isolated steady ellipse, shown as the dashed lines in figures 2 and 3, illustrate the applicability of this interpretation. For the horizontal ellipse and at distances greater than .03 chord lengths from the wake centerline, the calculations agree qualitatively with the measured velocity profiles, however close to the ellipse velocity differences of up to 10% are present. These differences are larger for the vertically oriented ellipse in figure 3, due to both the larger separation zone behind the ellipse and the decreased distance between the wake and the ellipse surface.

As the measurement station is moved downstream past x/c=1.20 the combination of the reduced airfoil wake velocity deficit and the increased interaction of the flow field of the ellipse with that of the airfoil make interpretation difficult. Therefore, only results for $x/c \leq 1.20$ will be discussed here. For the case of the steady horizontal ellipse (fig 2) the wake appears to be a fairly typical turbulent wake, with some asymmetry due primarily to the effect of the ellipse on the airfoil pressure distribution and boundary layers (1,2). Maximum velocity deficits range from 43% of the external velocity at x/c=1.025 to 20% at 1.2, indicating that these data describe the near wake, a region dominated by airfoil and boundary layer effects rather than by the similarity relations that control the far wake. This conclusion is reinforced by the fact that x/c=1.20 corresponds to 60 mean momentum thicknesses, much less than the 350-1000 that often define the start of the far wake (4,7).

For the case of the steady vertical ellipse (fig 3) the asymmetry of the wake is much greater, with the width at half maximum velocity deficit 3.8 times larger for the upper half of the wake than for the lower. As expected the wake is deflected upwards much more strongly by the vertical ellipse.

A second important characteristic of the steady wake is the mean Reynolds shear stress u'v'. Figure 4 shows profiles for the horizontal ellipse case described above. The stress is normalized by the square of the mean

external velocity. For clarity the profile for each sucessive value of x/c has been offset horizontally by $\overline{u'v'}$=.004. The asymmetry seen at x/c=1.025, where the maximum stress is 4.5 times larger below the centerline than above it, is reduced at x/c=1.2. Note the small values of $\overline{u'v'}$ outside of the airfoil wake, demonstating that the flow field of the elliptic cylinder, while nonuniform, is not highly turbulent. In the case of the steady vertical ellipse (fig 5), this property still holds above the wake and ahead of the ellipse (x/c<=1.1), but as the effect of the wake of the ellipse begins to be felt at x/c=1.2, noticeable turbulent shears are observed outside of the airfoil wake. The asymmetry is much greater for the case of the vertically oriented ellipse, with the ratio of the maximum $\overline{u'v'}$ above and below the wake centerline equal to 7.2 at x/c=1.025 and 1.9 and x/c=1.20. These numbers also show how the symmetric far wake is being slowly approached. Finally, in comparing the shear stress and mean velocity profiles, the region of large shears corresponds to that of large velocity deficit, in agreement with previous results (10).

Many of the features of the steady wake are preserved when the ellipse is rotated to produce unsteady flow. For example, the mean tangential velocity profiles at k=2 (fig 6), are qualitatively similar to those for the steady state (figures 2 and 3). At x/c=1.2, the vertical deflection of the minimum mean velocity is .014 chord, a value between the steady case deflections of .003 and .036. Again, the mean flow fields of the airfoil wake and the ellipse are distinct. Profiles for the other frequencies are qualitatively similar, but differ in detail. Near the trailing edge, at x/c=1.025, the differences are not significantly larger than the experimental accuracy, as is true for the mean boundary layer velocity profiles (2). The differences increase downstream, as maximum velocity deficits vary by up to 5% of U_e for x/c=1.2. Since the wake is not constrained to have zero velocity at a surface, as is the boundary layer, it is more sensitive to the large, frequency dependent increments of vertical velocity induced by the rotating ellipse.

The vertical velocity in the wake is shown for the same case in figure 7. Again, there is an offset of v=0.1 between profiles at sucessive x stations. Velocities above the centerline are quite small compared to those below, which are exposed to the full effect of the ellipse. For example, at x/c=1.025 the vertical velocity at y/c=-.03 is 5 times larger than the velocity at y/c=+.03. The vertical velocity is reduced after the ellipse axis is passed (x/c>=1.2), since the mean upwash ahead of the axis becomes a downwash behind it. The rapid variation in vertical velocity seen near the trailing edge rapidly disappears downstream, as the ellipse induced flow field dominates the wake.

The periodic unsteady velocity, given here by the fundamental harmonic of the ensemble average, may also be interpreted as a combination of a field due to the ellipse with that of the airfoil wake. Figure 8 shows profiles of $\langle u \rangle$ for the k=2 case. Each sucessive profile is offset by $\langle u \rangle / U_e$=0.05. Near the trailing edge, at x/c=1.025, the ellipse field is relatively uniform above and below the wake, with a much larger amplitude below. In the wake the contribution of the two boundary layers may be distinguished, separated by a minimum corresponding to the airfoil surface. The upper portion is similar to that observed in the boundary layer at x/c=0.94 (2). As the measurement station is moved downstream the unsteady wake amplitudes diffuse, obscuring the distinction between the upper and lower segments, while the amplitude due to the ellipse increases greatly, in particular below the centerline, so that the profile appears to be a smooth distribution, decreasing with distance from the ellipse, with only an S-shaped bump on the wake centerline. A similar process occurs for the vertical velocity (fig 9).

Phase lag distributions for the two velocity components are shown in figures 10 and 11. Outside of the wake, phase lags vary smoothly and increase with normal distance from the ellipse and with distance downstream of the airfoil. This corresponds roughly to propagation of disturbances from the ellipse and to downstream convection, respectively. In the wake the situation is more complex. Near the trailing edge there is a jump in tangential velocity phase lag of approximately 135°near the centerline. This jump is not well understood, but may be due to the different behaviors of the adverse pressure gradient upper surface boundary layer and the favorable pressure gradient lower surface boundary layer. As with the amplitudes, the phase jump diffuses downstream into a smaller 45 degree S-shaped bend. The vertical velocity phase has a much smaller jump near the trailing edge, which also is reduced at large x.

For a turbulent flow with a periodic excitation the Reynolds stresses, such as $\langle u'v' \rangle$, are defined so as to remove the contribution from the periodic component of the flow, uv. Using this definition the mean shear stress, $\overline{u'v'}$, distribution for k=2, as shown in figure 12, is qualitatively similar to the steady horizontal case of

figure 4. The major differences are a reduced asymmetry and an increased dissipation, most likely due to the increased mixing caused by the periodic velocities.

The mean turbulence intensities, $\overline{u'u'}$ and $\overline{v'v'}$, shown in figures 13 and 14 follow similar trends. $\overline{u'u'}$ has a minimum near the centerline at x/c= 1.025, resulting from the airfoil surface and viscous boundary layer sublayer, while the difference in maxima above and below the centerline refect the 2 boundary layers. The minimum of $\overline{v'v'}$ is much less pronounced, and in contrast to $\overline{u'u'}$ the maxima from the lower surface is larger than that from the upper surface. Both intensities dissipate downstream.

In unsteady flow the ensemble averaged turbulent stresses have time dependent components. Figures 15,16 and 17 show the amplitude of the fundamental harmonic of $\langle u'v' \rangle$, $\langle u'u' \rangle$ and $\langle v'v' \rangle$, respectively. Near the trailing edge all three have maxima both above and below a centerline minimum. The lower maximum is always stronger, with only $\langle u'u' \rangle$ having a strong peak above the centerline. The relative intensities of the three quantities agree with those measured in the upper surface boundary layer (2). As the measurement station is moved downstream the centerline minimum is retained, as is not true for either the mean stress or the periodic velocities. At x/c=1.2, the contribution from the ellipse to the amplitudes becomes relatively large, making interpretation more difficult.

At zero angle of attack profiles for the other frequencies, k=0.5 and 6.4, are qualitatively similar to those shown for k=2.0, but somewhat different in detail. Because of space limitations profiles are not presented here. As in the airfoil boundary layer, amplitudes of the periodic velocities decrease with increasing frequency. At x/c=1.025 $\langle u \rangle$ is 3 times larger at k=0.5 than at k=6.4, but at x/c=1.20 it is only 25% larger. Differences in phase lag due to frequency are primarily exhibited as an increase in the overall phase lag of the entire wake. An increase of 20 degrees in the phase lag of $\langle u \rangle$ occurs between k=0.5 and 2.0. Differences in the means of $\langle u'v' \rangle$ and $\langle u'u' \rangle$ due to frequency are less than 5%, while the amplitudes of the fundamental harmonic decrease with increasing frequency. This behavior parallels that seen in the boundary layer (2).

At k=0.5 data was taken at a Reynolds number of 1,450,000 in addition to 700,000. A comparison of the results reveals only minor differences. The most significant is a reduction in the normalized turbulence intensities and shear stress near the trailing edge. For example the maximum of the mean of $\langle u'v' \rangle$ at x/c=1.025 is 3.5 times smaller at the higher Reynolds number, but at x/c=1.2 this difference has largely vanished.

Wake profiles at the second position (10° angle of attack and a reduced ellipse - airfoil distance) are quite different from those at 0. Results will be given for the same frequency and Reynolds number given for α=0. The mean tangential velocity profiles, as seen in figure 18, are much broader, have a much larger velocity deficit at x/c=1.025, are more asymmetric, and have a larger vertical deflection. The initial wake thickness is 2.3 times larger at α=10° than at α=0, a result primarily of the thicker upper surface boundary layer (2). The maximum velocity deficit at α=10° is 80% of U_e, while at α=0 it is 50%. At x/c=1.025 the ratio of the upper and lower half thicknesses for α=0 is 2.0, while for α=10° it is 4.4. The deflection from the chordline is larger at α=10° than at α=0 for two reasons. At α=10° the flow must turn 10° more than at α=0 to become parallel to the freestream. Also, since the ellipse is closer to the wake at this position, a larger vertical velocity is induced.

As shown in figure 19, the mean normal velocity profile at x/c=1.025 has a sharp jump across the wake centerline of approximately 30% of the external u velocity. Above the jump the velocity is low, as required by the surface boundary condition on the airfoil, while below the jump the velocity is large, due to the upwash induced by the rotating ellipse. The steep gradient diffuses rapidly, as difference of only 5% of the external velocity remains at x/c=1.2.

The qualitative features of the unsteady components of the flow are less altered by the change in mean flow geometry than are the mean velocities. As shown in figure 20, the amplitude of $\langle u \rangle$ is still characterized by two peaks. The upper peak is quite broad, as it is a result of a thick boundary layer in a adverse pressure gradient (2). The lower peak is thinner, since it comes from a favorable pressure gradient boundary layer. Since the lower surface is closer to the ellipse, the unsteady amplitudes are larger, in this case by a factor of 4 at x/c=1.025. The lower peak rapidly broadens and appears to absorb the upper peak by x/c=1.2. As at α=0, the unsteady velocities deflect vertically with the mean velocity deficit, and have similar length scales. Phase lags, as seen in figure 21, are also dominated by a sharp peak from the lower surface boundary layer, which broadens by x/c=1.2 to form the characteristic S-shaped bump in the

smooth phase gradient of the ellipse induced flow field.

The mean turbulent shear stress, $\overline{u'v'}$, in figure 22, exhibits the same broad upper peak seen in the boundary layer data (2), while there is a sharp, narrow lower peak similar to that seen in the periodic velocity distribution (fig 20). Amplitudes are much larger than at α=0, with the upper maximum increasing from -.00074 to -.0027, and the lower from .0024 to 0.0038, at x/c=1.025. The fundamental harmonic of $\langle u'v' \rangle$, shown in figure 23, has the characteristic double peak near the trailing edge. As at α=0, a triple peak has developed by x/c=1.1, for as yet undetermined reasons.

Because of space limitations, as before data at the other frequencies tested at α=10 degrees are omitted, but as at α=0, differences due to frequency involve the details of the flow fields more than the qualitative features emphasized in this paper.

Summary and Conclusions

On the basis of a preliminary examination of these results, several broad conclusions may be drawn regarding the nature of the flow field, the influence of the test parameters and the interdependence of the components of the flow.

In the region of the wake studied, within 0 to 0.2 airfoil chord or roughly 100 mean momentum thicknesses downstream of the trailing edge, flow characteristics are highly dependent on the airfoil and its boundary layers. This is demonstrated by the high degree of asymmetry present in the profiles for the mean, periodic, and turbulent velocities. Profiles measured at x/c=1.025 are quite similar in many respects to those measured in the upper surface boundary layer at x/c=0.94. The wake becomes more symmetric downstream as the sharp gradients diffuse. Significant asymmetries do however persist beyond x/c=1.20.

Four parameters may be varied in this experiment: Reynolds number, reduced frequency, geometric angle of attack, and distributed angle of attack (due to the location of the ellipse axis relative to the airfoil). Changes in the airfoil boundary layers and pressure distributions due to increased angle of attack are reflected in the wake as increases in the mean velocity deficits, unsteady velocity and turbulent stress amplitudes, gradients of the phase lag and wake thicknesses. Vertical deflection of the wake and gradients of the mean vertical velocity increase as the distributed angle of attack is increased. The mean velocity and turbulent stress profiles are not significantly altered by changes in the reduced frequency, while the periodic amplitudes decrease as expected when frequency increases. These differences due to frequency are reduced downstream of the trailing edge. Based on the limited data studied to date, the main effect of doubling the Reynolds number to 1,450,000 is a reduction of the turbulent stresses near the trailing edge.

It is suggested that the flow field may be interpreted in several ways. One is as a combination of the wake of the airfoil with the nonuniform flow directly produced by the ellipse. Away from the surface of the ellipse, its field may be approximated by a potential flow about the ellipse. The qualitative features of such a flow are similar to those measured outside of the airfoil wake. This approximation begins to break down as the departure from a uniform flow becomes larger such as when the airfoil angle of attack is high, the ellipse major axis is vertical, or when the airfoil wake approaches the ellipse surface or its wake.

A second interpretation of the flow is as a superposition of a mean flow, a periodic unsteady flow and an aperiodic or turbulent flow. Mean and periodic pressures on the airfoil surface were found to be largely decoupled. The mean pressures depend primarily on airfoil geometric angle of attack and the mean distributed angle of attack, while the periodic pressures depend primarily on the reduced frequency and the periodic component of the distributed angle of attack (1,15). Similarly mean velocity and turbulent stress profiles showed little dependence on reduced frequency at zero angle of attack, while the periodic profiles appeared to approach similar profiles independent of the mean parameters and profiles for high frequency (2). On the contrary however for low frequencies (k<=1) and high adverse gradients (i.e. at α=10°), a coupling was observed between the mean velocity, the periodic velocity and the mean turbulent shear stress.

In the wake very near to the trailing edge (x/c=1.025) this behavior is still present. Further downstream the situaion becomes less clear. As described above, the mean velocity and turbulent stresses are relatively independent of frequency, while the periodic amplitudes are significantly altered. The reverse is not true here, as the periodic component of the flow has a large dependence on the mean parameters. This difference from the behavior in the boundary layer is not understood in detail but is probably in

part due to the difference in boundary conditions. It is therefore difficult to demonstrate any decoupling of the mean, periodic and turbulent flow field components downstream of the trailing edge, based on the current data.

Acknowledgement

This research was sponsored by the U.S. Air Force Office of Scientific Research under grant AFOSR-80-0282. Dr. Michael S. Francis was the contract monitor.

References

1) Lorber,P.F.,and Covert,E.E., "Unsteady Airfoil Pressures Produced by Periodic Aerodynamic Interference," AIAA Journal,Vol.20,1982,pp.1153-1159.

2) Covert,E.E.,and Lorber,P.F., "Unsteady Turbulent Boundary Layers in Adverse Pressure Gradients," AIAA paper 82-0966, June 1982, submitted to the AIAA Journal.

3) Daniels,P.G., "On the Unsteady Kutta Condition," Q.Jl.Mech.appl.Math, Vol 31, Part 1, 1978, pp.49-75.

4) Ramaprian,B.R., Patel,V.C., and Sastry,M.S., "The Symmetric Turbulent Wake of a Flat Plate," AIAA Journal, Vol. 20, 1982, pp.1228-1235.

5) Hah,C., and Lakshminarayana,B., "Measurement and Prediction of Mean Velocity and Turbulence Structure in the Near Wake of an Airfoil," J.Fluid.Mech., Vol 115, 1982, pp.251-282.

6) Patel, V.C., "Two Dimensional wakes," Data Evaluation Report, 1980-81 AFOSR-HTTM-Stanford Conference on Complex Turbulent Flows, 1980.

7) Patel, V.C. and Scheuerer,G., "Calculation of Two-dimensional Near and Far Wakes," AIAA Journal, Vol. 20, 1982, pp.900-907.

8) Rhie,C.M. and Chow, W.L., "A Numerical Study of the Turbulent Flow Past an Isolated Airfoil with Trailing Edge Separation," AIAA paper 82-0998, June 1982.

9) Reynolds,B., Lakshminarayana,B. and Ravindranath,A., "Characteristics of the Near Wake of a Compressor or Fan Rotor Blade," AIAA Journal, Vol 17, 1979, pp.959-967.

10) Hah,C. and Lakshminarayana,B., "Prediction of Two and Three-dimensional Asymmetrical Turbulent Wakes, Including Curvature and Rotation Effects," AIAA Journal, Vol.18, 1980, pp 1196-1204.

11) Satyanarayana,B. "Unsteady Wake Measurements of Airfoils and Cascades," AIAA Journal, Vol.15, 1977, pp.613-618.

12) Ho,C.M. and Chen,S.H., "Unsteady Wake of a Plunging Airfoil," AIAA paper 80-1446, July 1980.

13) Ho,C.M. and Chen,S.H., "Unsteady Kutta Condition of a Plunging Airfoil," in "Unsteady Turbulent Shear Flows," edited by R.Michel, J.Cousteix and R.Houdeville, Springer-Verlag, Berlin, 1981.

14) DeRuyck,J. and Hirsch,C., "Instantaneous Turbulence Profiles in the Wake of an Oscillating Airfoil," AIAA paper 82-0353, Jan. 1982.

15) Lorber,P.F., and Covert,E.E., "Additional Results of a Study of Unsteady Airfoil Surface Pressures and Turbulent Boundary Layers," AFOSR-TR-81-0848-TR, Nov. 1981.

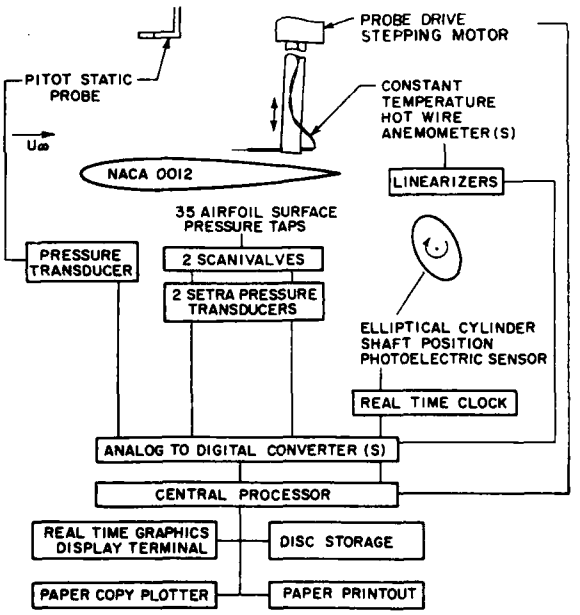

Fig.1 Instrumentation Diagram

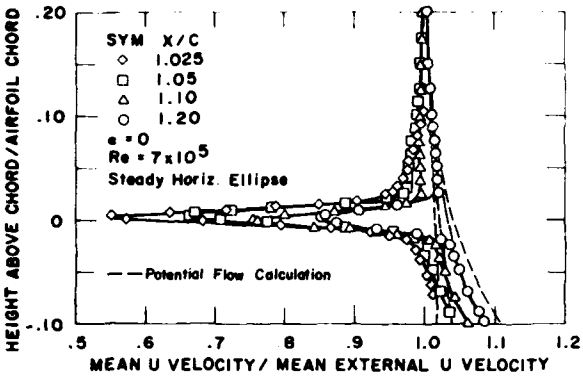

Fig.2 Mean Tangential Velocity

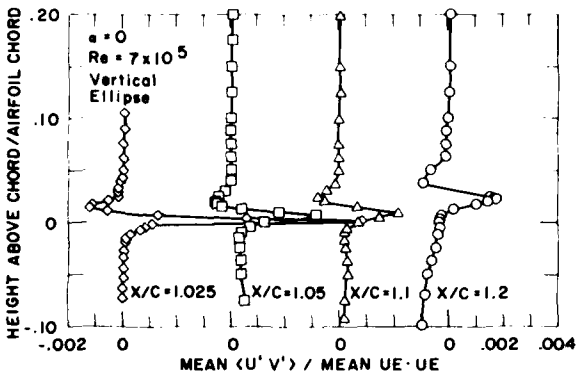

Fig.5 Mean Turbulent Shear Stress

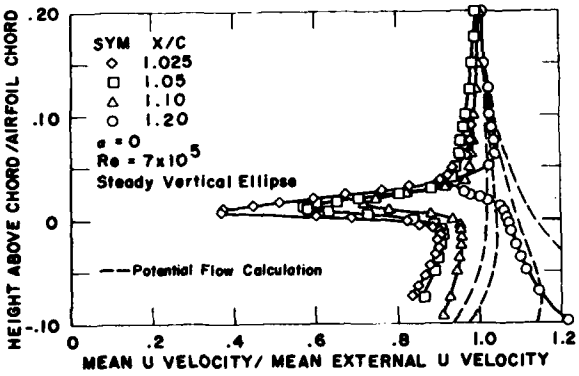

Fig.3 Mean Tangential Velocity

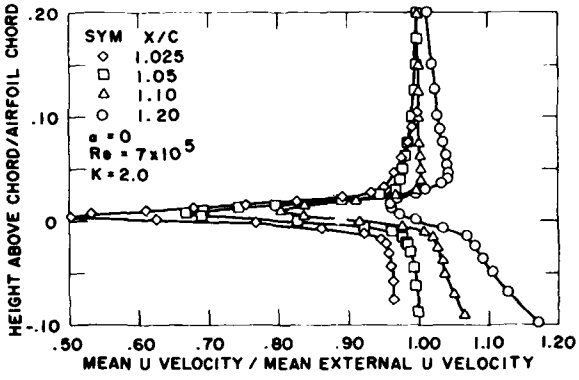

Fig.6 Mean Tangential Velocity

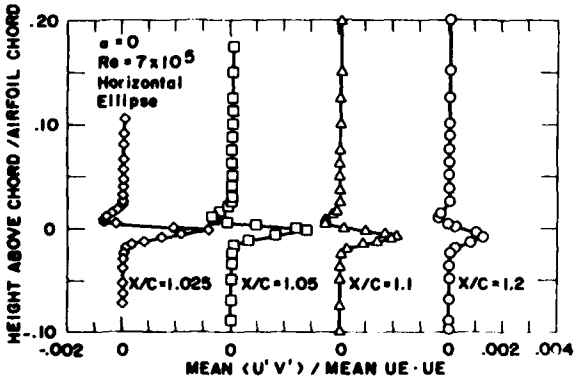

Fig.4 Mean Turbulent Shear Stress

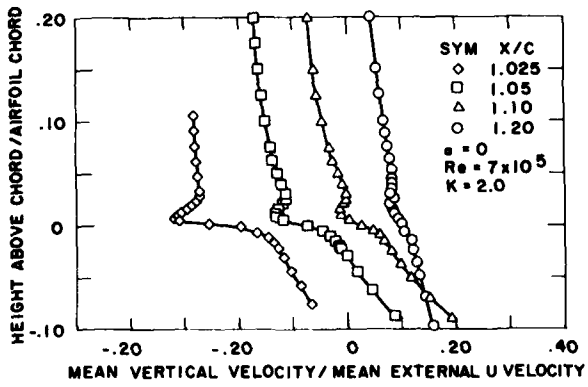

Fig.7 Mean Normal Velocity

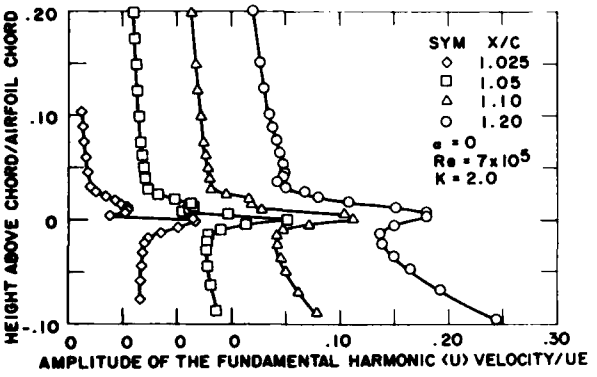

Fig.8 Periodic Tangential Velocity Amplitude

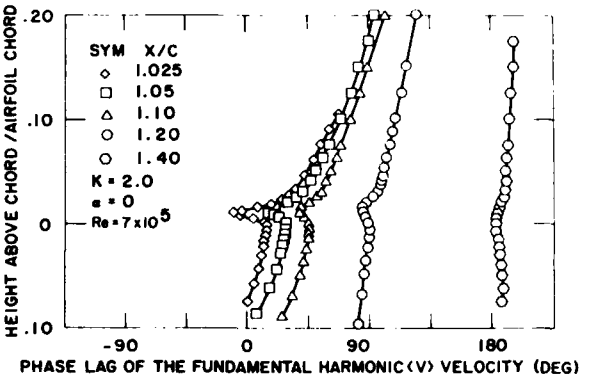

Fig.11 Periodic Normal Velocity Phase

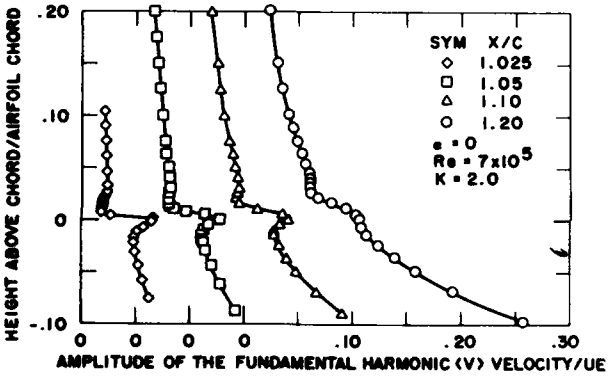

Fig.9 Periodic Normal Velocity Amplitude

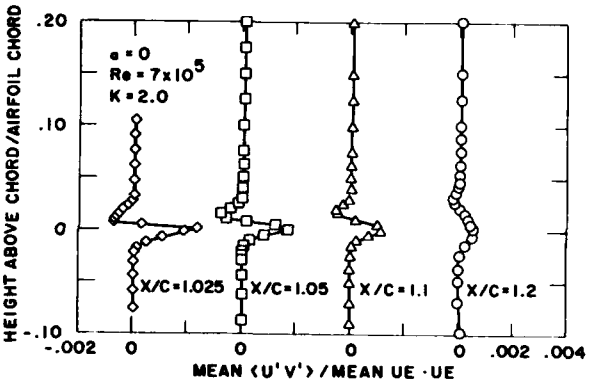

Fig.12 Mean Turbulent Shear Stress

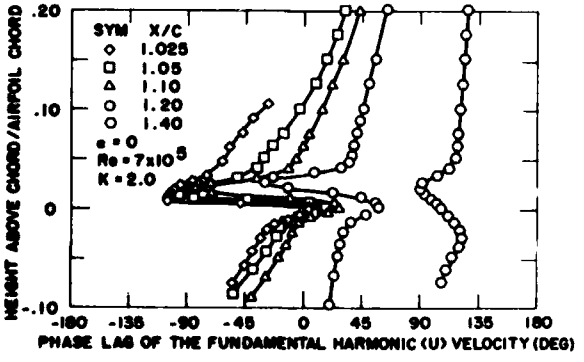

Fig.10 Periodic Tangential Velocity Phase

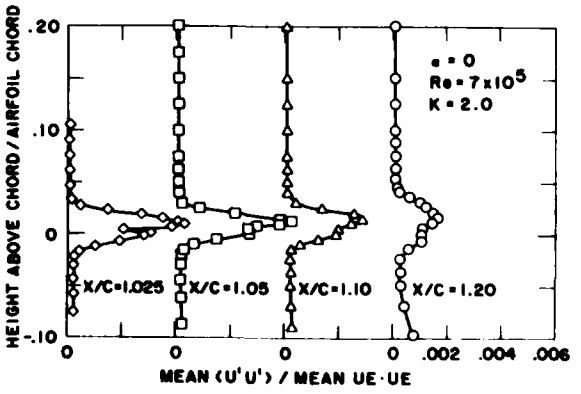

Fig.13 Mean Tangential Turbulence Intensity

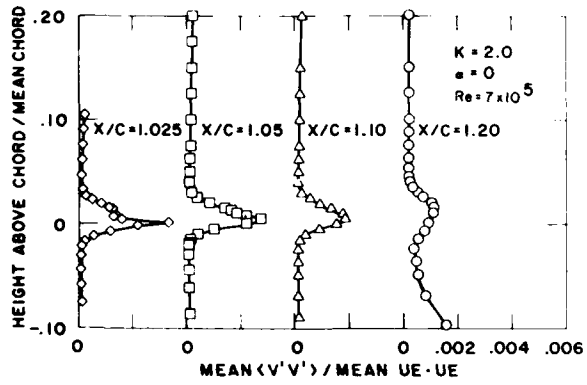

Fig.14 Mean Normal Turbulence Intensity

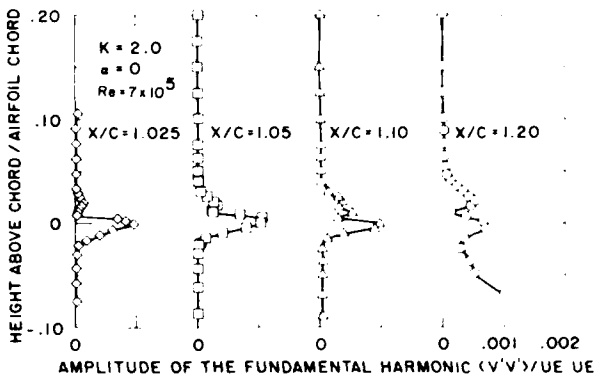

Fig.17 Periodic Normal Turbulence Intensity

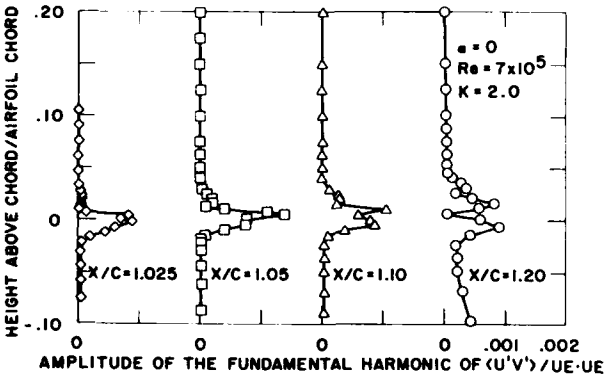

Fig.15 Periodic Turbulent Shear Stress

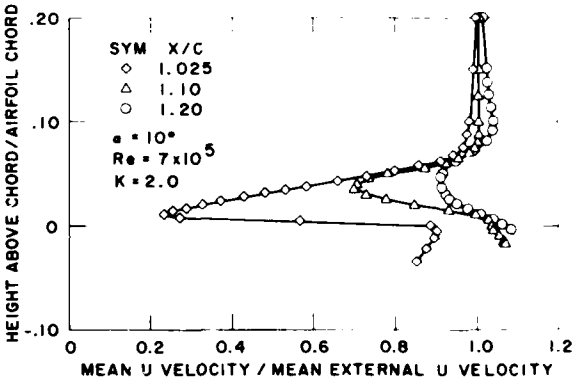

Fig.19 Mean Normal Velocity

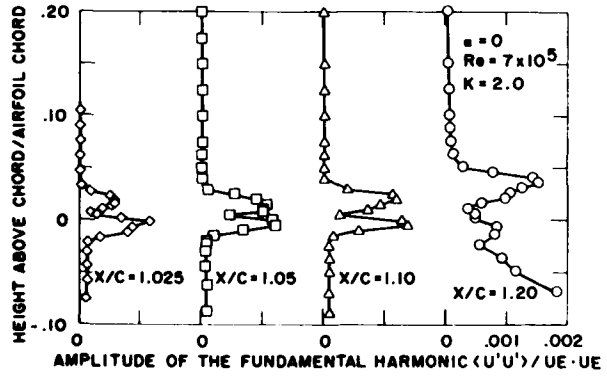

Fig.16 Periodic Tangential Turbulence Intensity

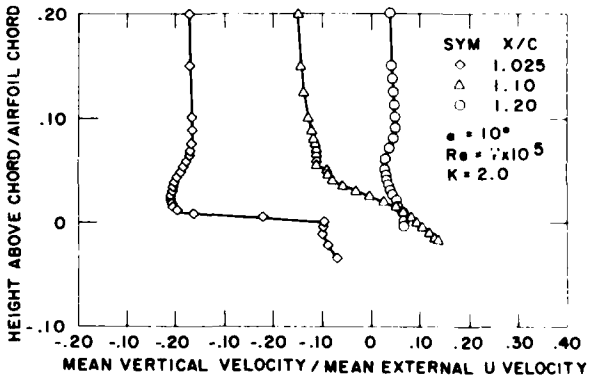

Fig.18 Mean Tangential Velocity

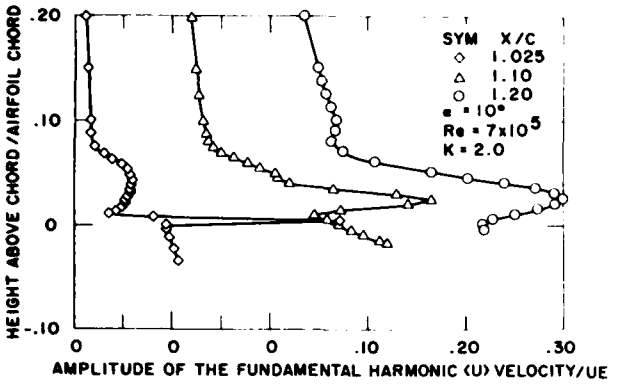

Fig.20 Periodic Tangential Velocity Amplitude

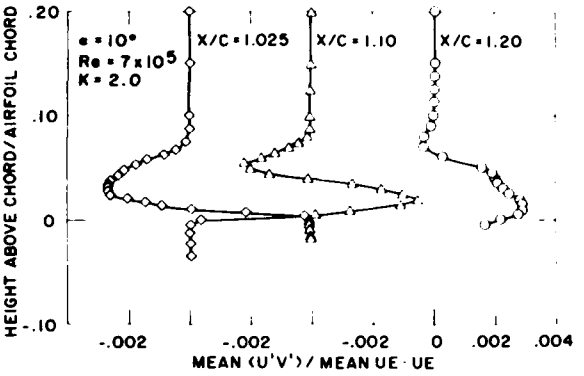

Fig.22 Mean Turbulent Shear Stress

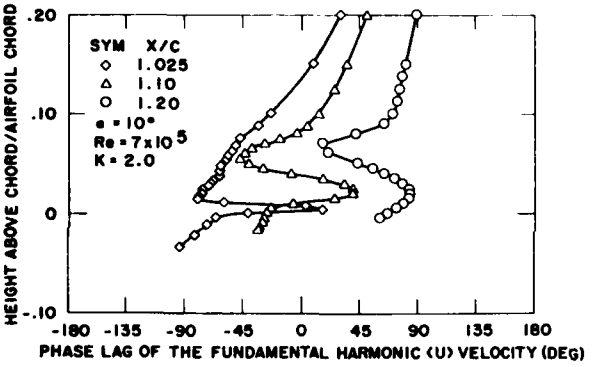

Fig.21 Periodic Tangential Velocity Phase

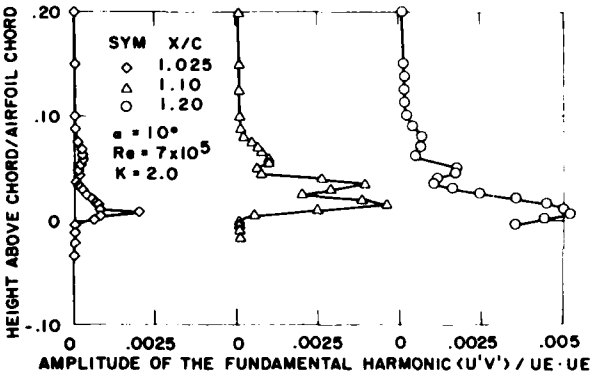

Fig.23 Periodic Turbulent Shear Stress

END

FILMED

3-84

DTIC